

Biotic and abiotic products of Mn(II) oxidation by spores of the marine *Bacillus* sp. strain SG-1

JOHN R. BARGAR,^{*,1} BRADLEY M. TEBO,² UWE BERGMANN,¹ SAMUEL M. WEBB,¹ PIETER GLATZEL,³
VAN Q. CHIU,² AND MARIO VILLALOBOS⁴

¹Stanford Synchrotron Radiation Laboratory, SLAC, Stanford, California 94309, U.S.A.

²Marine Biology Research Division, Scripps Institution of Oceanography, 9500 Gilman Dr., La Jolla, California 92093-0202, U.S.A.

³Department of Inorganic Chemistry and Catalysis, Utrecht University, 3584 CA Utrecht, The Netherlands

⁴Environmental Biogeochemistry Group, LAFQA, Instituto de Geografía, National Autonomous University of Mexico, Circuito Exterior, Ciudad Universitaria, Coyoacán, 04510, D.F., Mexico

ABSTRACT

Bacterial Mn(II) oxidization by spores of *Bacillus*, sp. strain SG-1 has been systematically probed over the time scale 0.22 to 77 days under in-situ conditions and at differing Mn(II) concentrations. Three complementary techniques, K-edge X-ray absorption near-edge spectroscopy (XANES), X-ray emission spectroscopy (XES), and in-situ synchrotron radiation-based X-ray diffraction (SR-XRD), have been utilized to examine time-dependent changes in Mn oxidation state, local-, and long-range structure in amorphous, crystalline, cell-bound, and solute Mn species. The primary solid biogenic product of Mn(II) oxidation is an X-ray amorphous oxide similar to δ -MnO₂, which has a Mn oxidation state between 3.7 and 4.0. Reaction of Mn(II) with the primary biogenic oxide results in the production of abiotic secondary products, feitknechtite or a 10 Å Na phyllosmanganate. The identity of the secondary product depends upon the Mn(II) concentration as described by thermodynamic relations. A decrease in the dissolved Mn(II) concentration is followed by mineralogic transformation of the secondary products. Thus, Mn(II) appears to act as a reductant toward the biogenic oxide and to control the stability of secondary reaction products. Mineralogic changes similar to these are likely to be commonplace in natural settings where bacterial Mn(II) oxidation is occurring and may liberate sorbed metal ions or alter the rates of important Mn oxide surface-mediated processes such as the degradation of organic molecules. It is plausible that microbes may exploit such mineral transformation reactions to indirectly control specific chemical conditions in the vicinity of the cell.

INTRODUCTION

Manganese oxides are abundant as nanoparticulate grains and grain coatings in the oxic and suboxic zones of freshwater and marine environments (Burns 1976; Burns and Burns 1979; Jenne 1967; McKenzie 1980). Oxidation of Mn(II) in these near-surface environments is believed to be dominated by microbial action (Fuller and Harvey 2000; Harvey and Fuller 1998; Marble et al. 1999; Tebo 1991; Tebo et al. 1984), and bacteria are thus believed to be major drivers of the global Mn cycle. Manganese oxides are known to have high sorptive capacities for a wide variety of metal ions (see review by Tebo et al. 2004), including Fe(II), Co(II), Ni(II), Cu(II), Zn(II), actinides, and P-block metals such as Pb(II) (Jenne 1967; McKenzie 1980; Nelson et al. 1999; O'Reilly and Hochella 2003). The affinity for these metals allow Mn oxides to exert considerable influence on trace metal speciation in aquifers, oceans, and biofilms, even when present as minor components of the system (e.g., Duff et al. 1999; Haack and Warren 2003). Manganese oxides are among the strongest of oxidants in the environment and degrade or oxidize many organic and inorganic compounds, including humic and fulvic

acids, aromatic hydrocarbons, Cr(III), Co(II), and hydrogen sulfide (Huang 1991; Jenne 1967; Post 1999). In this fashion, Mn oxides participate directly in global cycling of micronutrients, contaminants, carbon, nitrogen, and sulfur. The need to deepen our understanding of these important biogeochemical cycles demands greater knowledge of bacterial Mn(II) oxidation processes, their mechanisms, and products. Furthermore, such knowledge is requisite to harnessing these natural processes for technological applications such as in situ remediation of contaminated ground water.

Central to these puzzles are the pathways by which bacteria oxidize Mn(II) and precipitate it as a solid, and the reactivity and fate of these bacteriogenic Mn oxide products. Aging and mineralogic transformations of the bacteriogenic oxides are likely to occur, due to the rapid kinetics of Mn(IV) precipitation (which may lead to metastable phases) and the complex stability relationships that occur between Mn oxide phases at near-neutral pH (Mandernack et al. 1995). In addition, autocatalytic (abiotic) oxidation of Mn(II) is expected to occur at the surfaces of bacteriogenic Mn(III,IV) oxides. All such transformations will be important in the environment because they involve the exchange of cations and electrons with the local environment. Furthermore, such reactions could be utilized by bacteria to indirectly poison

*E-mail: bargar@ssrl.slac.stanford.edu

the compositions of their microenvironments.

Bacterial Mn(II) oxidation has been the subject of several previous investigations. Hastings and Emerson (1986) reported the occurrence of hausmannite (Mn_3O_4), which they interpreted as an intermediate in the oxidation of Mn(II) by spores of marine *Bacillus* sp. strain SG-1. Mann et al. (1988) also reported hausmannite as an SG-1 oxidation product at 25 mM Mn(II). Pecher et al. (2003) reported the presence of Mn(III) in contact with SG-1 spores during oxidation of 10 mM Mn(II) by SG-1. In contrast to these observations, Mandernack et al. (1995) concluded that Mn(II) is oxidized directly to Mn(IV) without an intermediate. These authors further noted that, at pH = 8 (the value at which SG-1 obtains its maximum oxidizing activity) and Mn(II) concentrations greater than about 10^{-7} M, hausmannite, α -, and γ -MnOOH are stable with respect to transformation into MnO_2 , and thus should not be assigned as intermediates. Bargar et al. (2000) reported the absence of detectable Mn(III) signatures during the first 9 hours of Mn(II) oxidation by SG-1 spores. Desiccated biogenic Mn oxides produced by *Pseudomonas putida*, strain MnB1, were studied by Villalobos et al. (2003) and found to be 7 Å hexagonal phyllophanes (layer Mn oxides) with an Mn oxidation state of 3.9. Studies of the genes encoding the putative Mn(II)-oxidizing proteins in different bacteria strongly suggest that Mn(II) oxidation is accomplished by a multicopper oxidase (Tebo et al. 2004; Tebo et al. 1997), which typically catalyze one-electron transfer reactions. If true, then complexed Mn(III) would be expected to occur as a reaction intermediate, which could be enzymatically oxidized to Mn(IV). Recently, Webb et al. (2004) have reported direct observation of enzyme-bound Mn(III) intermediates during Mn(II) oxidation by SG-1.

Consideration of these studies does not lead directly to a comprehensive mechanistic picture of bacterial Mn(II) oxidation due to the differences in techniques and time scales utilized. A further complication is the poor crystallinity of natural Mn oxides and the relatively sensitive dependence of Mn oxide structure and oxidation state on pH, hydration state, and solution composition (Tebo et al. 2004). To develop a comprehensive picture of the overall bacterial Mn(II) oxidation reaction, it is essential to utilize techniques that can probe Mn oxidation states directly in amorphous and crystalline phases under in-situ conditions. The present work expands on these previous studies by systematically examining the products of Mn(II) oxidation by SG-1 spores over time scales of 0 to 77 days under fully hydrated conditions using three complementary techniques, K-edge XANES, XES, and SR-XRD, which allow the determination of Mn oxidation state and phase identity in wet, unaltered biooxide/cell mixtures. Key questions that we seek to address in this paper are the formation, occurrence, and transformations of bacteriogenic Mn oxides on the bulk scale.

EXPERIMENTAL METHODS

Preparation of biogenic Mn oxides

The marine Mn(II)-oxidizing *Bacillus* species strain SG-1 was isolated from an enrichment culture inoculated with sediments collected off Scripps pier (Nealson and Ford 1980). For SG-1, it is the spores, and not the vegetative cells, that oxidize Mn(II). SG-1 was grown on K medium (0.5 g/L yeast extract, 2 g/L peptone, 10 mM HEPES buffer, 100 μM $\text{MnCl}_2 \cdot 4\text{H}_2\text{O}$ in 75% strength natural seawater) until the culture was fully sporulated (~5 days). The spores were purified according to published procedures (Rosson and Nealson 1982) except that before the final Milli-

Q water washes, the spores also were reacted with 0.2 mM ascorbate in 10 mM HEPES buffer (pH = 7.8) to remove Mn(III,IV) oxides formed during culturing. Spore concentrations were determined by direct counting using a phase-contrast light microscope and a Petroff-Hauser counting chamber. Spores were stored frozen at -20°C until used. Prior to use, the spores were thawed on ice and dispersed using a tissue homogenizer.

SG-1 spores were incubated in 10 μM or 1 mM Mn(II) (added as $\text{MnCl}_2 \cdot 4\text{H}_2\text{O}$) in 50 mM NaCl/10 mM HEPES buffer (final pH = 7.7–7.8) in 8 L glass carboys on magnetic stirrers (10 μM) or in 1 L Erlenmeyer flasks on a rotary shaker (1 mM), all being gently bubbled with O_2 to maintain generally oxic conditions. The experiments were started by adding 1.3×10^{10} spores to each incubation vessel resulting in 2.2×10^6 and 1.3×10^7 spores/mL for the 10 μM and 1 mM incubations, respectively. For each time point, the entire contents of one of each Mn(II) concentration series was harvested (except for the last two time points when only $1/2$ of the content of the last vessel at each concentration was harvested at each time point) by centrifugation at 4°C . The cell/oxide pellets were stored under 10 mL of their original medium at -20°C until analysis. For the 10 μM experiment, a second aliquot of ~10 μM Mn(II) was added after the 4th time point (1.97 days). The concentration of Mn(II) was measured colorimetrically using the formaldoxime method (Brewer and Spencer 1971). Results are summarized in Table 1. A second short-term (2 h) synthesis of biogenic Mn oxide was conducted for the 1 mM Mn(II) concentration as a separate experiment using similar methods, except the final spore concentration was 1.1×10^7 spores/mL. A third experiment with 1 mM Mn(II) was conducted with the Mn(II) concentration maintained between 0.68 and 0.96 mM [Mn(II)] (defined as the concentration of all soluble Mn(II) species) for up to 9 days by measuring Mn(II) concentration at each time point and adding back the amount of Mn(II) that was removed.

Abiotic control samples were prepared in two fashions to test the possibility that Mn(II) was oxidized by reaction with bio-oxides. In one, 200 mL of 0.01 g/L of fresh δ - MnO_2 (i.e., less than two months old, stored in water at 3°C , prepared following the procedure described by Murray 1974), was added to a 50 mM NaCl solution containing 10 mM HEPES. 100 μM MnCl_2 was added and the suspension was rotated end-over-end at room temperature for 12 and 21.5 hours. O_2 bubbling was not performed because of the emphasis on Mn oxides as oxidants, the excess of dissolved O_2 relative to Mn(II), and the presence of ~30 mL air head space. The solid was separated from solution by filtration through an 0.1 μm filter membrane, which was immediately loaded into a sample holder and maintained moist for XANES analysis. In the second preparation, 0.4 g/L fresh δ - MnO_2 was reacted with 1 mM MnCl_2 and 10 mM HEPES (bubbled with O_2), and agitated on a shaker table at room temperature.

In-situ synchrotron-based x-ray diffraction (SR-XRD)

Spore/oxide-paste mixtures were loaded into transmission sample XRD cells having polycarbonate windows to prevent desiccation of the sample and to enforce a well-defined slab geometry, or in to a 0.5 mm deep dish-style reflection sample holder (silicon or aluminum) having a hemispherical Mylar window to prevent desiccation. XRD intensity data were collected in bisecting geometry at room temperature at SSRL beam line 2-1 using a Bircan photomultiplier tube detector equipped with Soller slits to reject air scattering and improve angular resolution. A single-channel analyzer was used to window on the elastic scatter peak. X-ray energy was set to 10 KeV using a Si(111) double-crystal monochromator. Wavelength and 2θ calibrations were maintained by frequently measuring intensity data from an aluminum foil (transmission geometry) or LaB_6 powder (reflection geometry). Wavelength was 1.2404 (± 0.001) Å. A platinum-coated toroidal focusing mirror was used to reject X-rays with energy >11 KeV and to produce a focused beam of dimensions $\sim 1 \times 4$ mm. The typical step size was 0.04 degrees. Transmission data were corrected for θ -dependent attenuation of incident and scattered X-rays. Separate XRD patterns were collected for the empty cell, a water-filled cell, and clean spores, and were then subtracted out of the transmission sample spectra, allowing the scattering arising from the spores and reaction products to be defined clearly. This subtraction procedure could not be performed for reflectance XRD data because of differences in the depth of penetration of the scattering medium in the water-filled cell and the samples. It was thus necessary to remove Kapton and water scattering by fitting the associated peaks with Gaussian peaks at positions determined from measurements of the empty cell, water-loaded cell, and clean, wet spore-loaded cell. Scattering from spores is present as a small peak located at $15.4^\circ 2\theta$ (width 4° FWHM) on the low angle side of the Kapton peak. Because of its small size and overlap by the Kapton peak, it was not possible to define the spore scattering peak accurately in the reflectance data, and it was effectively removed by the fitting procedure for reflectance data. Results are presented in Table 2.

TABLE 1. Sample conditions for Mn(II)+SG-1 spore incubation experiments. [Mn(II)] is the sum of all Mn(II) species in solution at the end of the experiment, expressed in terms of molarity

10 μM Mn(II)											
Reaction Time (d):	0	0.22	0.45	0.85	1.97	1.98 \ddagger	4.00	7.70	12.7	27.8	77
Mn(II) added*, moles $\times 10^{-6}$	56.9	56.9	56.9	56.9	56.9	113.9	113.9	113.9	113.9	113.9	113.9
[Mn(II)] _t (μ M)	9.49	9.04	7.73	5.58	1.24	10.73	3.38	0.25	0.14	0.09	NM
1 mM Mn(II), single addition at start											
Reaction Time (d):	0	0.08 \dagger	0.22	0.45	0.85	1.97	4.00	7.70	12.7	27.8	77
Mn(II) added*, moles $\times 10^{-3}$	1.0	1.0	1.0	1.0	1.0	1.0	1.0	1.0	1.0	1.0	1.0
[Mn(II)] _t (mM)	NM	NM	0.981	0.948	0.893	0.668	0.322	0.037	0.0001	0.0001	NM
1 mM Mn(II), maintained throughout experiment by repeated additions											
Reaction Time (d):	0	0.04	0.13	0.25	0.5	0.96	2.00	4.00	9.00		
Mn(II) added*, mmoles	0	7.9	7.9	7.9	7.9	7.9	7.9	8.3	8.6		
[Mn(II)] _t (mM)	NM	0.96	0.95	0.96	0.96	0.94	0.76	0.68	0.82		

* Cumulative sum from start of reaction.

 \dagger This time point was conducted as a separate experiment (see Materials and Methods). ND = Not measured. \ddagger XANES, XES, and XRD analyses were not performed on this point.

X-ray emission spectroscopy

X-ray emission spectroscopy (XES) measurements were performed at APS-BioCAT undulator beamline 18ID using a cryogenically cooled Si(111) double-crystal monochromator operated at 10 keV excitation energy. The beam had 0.3 mm vertical by 1 mm horizontal dimensions. The spectrometer used for $K\beta$ XES experiments had a FWHM energy resolution of <1 eV, and is described in detail elsewhere (Bergmann and Cramer 1998). Calibration of the emission energy was obtained by assigning the first moment (using an energy interval from 6485 eV to 6495 eV) of a Mn_2O_3 (solid sample) spectrum to 6490.4 eV (Visser et al. 2001). During data collection, sample solutions were kept in holders sealed by thin Kapton windows in an Oxford CF1208 cryostat at temperatures of <70 K under vacuum. Spectra were normalized by dividing the recorded fluorescence intensity by I_0 . Samples were exposed to the beam only during data acquisition to minimize beam damage. To address possible Mn photo-reduction from the intense X-ray beam, the following protocol was imposed: three subsequent scans were performed in the order A B A. Scan A was a short scan in the energy range of the main peak ($K\beta_{1,3}$), which is most indicative of radiation damage (Messinger et al. 2001). Its energy range is from 6487 to 6495 eV with an exposure time of 1 s per step and 41 s total. Scan B has a larger energy range from 6468 to 6506 eV, which includes $K\beta'$ and a total exposure time of 225 s. For the 6 and 11.8 hour spore samples, insignificant shifts of the main line due to photo-reduction were observed, i.e., the energy shifts were within the error bars given in the quantitative analyses.

Energy shifts in the $K\beta_{1,3}$ emission were quantified using a 1^{st} -moment analysis, which provides an accuracy of ± 0.01 eV (Messinger et al. 2001; Visser et al. 2001). Percent-composition analyses were performed by: linear least-squares combinations of emission spectra from models, and by using the first moments from the sample spectra according to: $P(X) = [1^{st}\text{-moment}(X) - 1^{st}\text{-moment}(4.0\text{ d incubation at } 10\ \mu\text{M})] / [1^{st}\text{-moment}(MnCl_2) - 1^{st}\text{-moment}(4.0\text{ d incubation at } 10\ \mu\text{M})]$. Error for these analyses is estimated at ca $\pm 1\%$ by taking the difference between the results from these two approaches (fits A and B in Table 3). Bulk Mn oxidation states were calculated from linear combination fits of $MnCl_2$, Mn_2O_3 , and the 4.0 d biooxide sample, for which the oxidation state was found to be 3.74. Uncertainty for bulk oxidation states relative to one-another is estimated at ± 0.02 , based on the 1% error estimated for percent-composition analyses. Absolute accuracies of bulk oxidation states are dominated by the assignment for the 4.0 d sample, and are estimated to be $\sim \pm 0.09$ (corresponding to a 5% error for percent-composition analyses).

Mn K-edge XANES measurements

Wet cell/Mn oxide pastes were loaded into Teflon sample holders with kapton windows. Unfocused XANES spectra were measured at room temperature at the Stanford Synchrotron Radiation Laboratory (SSRL) beam line 4-3 in transmission mode and simultaneously using a Lytle-type ionization chamber and Cr X-ray filters. A variable-exit Si(220) double-crystal monochromator was used detuned to attenuate harmonic intensity. The energy bandwidth was 0.67 eV at full width, half maximum (FWHM). Energy calibration was monitored by use of metallic Mn (6539.0 eV) and/or the pre-edge peak of $KMnO_4$ (6543.34 eV). Total beam intensity was approximately 2×10^{11} photons/s, which illuminated a sample volume of $2 \times 20 \times 1$ mm. Multi-hour exposure tests provided no evidence that the incident X-ray beam was reducing Mn(IV) to Mn(II).

Spectra were background-subtracted, normalized, and fit with linear combinations of component spectra using EXAFSPAK (George 1993). Transmission spectra were used whenever possible due to the presence of self-absorption effects in fluorescence data. When it was necessary to use fluorescence spectra, they were

TABLE 2. *d*-spacings for major reflections observed by X-ray diffraction

Sample	Observed <i>d</i> -spacings (Å)
10 μM Mn(II)	
0.22 d	–
0.45 d	–
0.85 d	–
1.97 d	10.15, 5.08
4.00 d	10.15, 5.08
7.70 d	10.15, 5.08, 3.38
12.70 d	10.15, 5.08, 3.38
27.80 d	10.15, 5.08, 3.38
77.0 d	8.85
1 mM Mn(II) Single addition at start of reaction	
0.22 d	–
0.45 d	–
0.85 d	–
1.97 d	4.61, 2.69 (Feitknechtite)
4.00 d	4.61, 2.69 (Feitknechtite)
7.70 d	4.61, 2.69 (Feitknechtite)
12.70 d	4.61, 2.69 (Feitknechtite) 10.15, 5.08, 3.38
27.80 d	4.61, 2.69 (Feitknechtite) 10.15, 5.08, 3.38
77.0 d	4.61, 2.69 (Feitknechtite) 10.15, 5.08, 3.38
1 mM Mn(II) Maintained throughout experiment by repeated additions.	
0.41 d	–
0.25 d	4.61 (Feitknechtite, at detection limit)
0.96 d	4.61, 2.69 (Feitknechtite)
2.00 d	4.61, 2.69 (Feitknechtite)
4.00 d	4.61, 2.69 (Feitknechtite)
9.00 d	4.61, 2.69 (Feitknechtite)

corrected for self-absorbance using SIXPACK (Webb 2003). Binding energies were allowed to float during fits by amounts not exceeding 0.25 eV. Up to four components were utilized for final fits: Mn(II) adsorbed to spores, clean spores [which contain intracellular Mn(II)], δ - MnO_2 , and synthetic triclinic Na birnessite ($Na_{0.3}Mn_{0.7}Mn_{0.3}O_2$) described previously (Villalobos et al. 2003). δ - MnO_2 was synthesized according to the method of Murray (1974), and had a Mn oxidation state of 3.84 ± 0.06 (idometric titration). SR-XRD patterns of the wet δ - MnO_2 (not shown) showed weak and strongly asymmetric (*hk*) peaks at 2.45 and 1.41 Å, and a broad (001) peak at 7.2 Å (weakest line). This pattern is in excellent agreement with that published by Villalobos et al. (2003), which was described as a turbostratically disordered hexagonal phyllosilicate, having only two or three layers stacked along the *c* axis. Other spectra utilized as references included: synthetic manganite (γ - $MnOOH$, synthesized by A. Stone), groutite (α - $MnOOH$, Roberts Mine, Minnesota), synthetic feitknechtite (β - $MnOOH$), bixbyite ($(Mn,Fe)_2O_3$, Thomas Mtn., Utah), synthetic hausmannite (Mn_3O_4), aqueous Mn(III)pyrophosphate [assumed to be $MnHP_2O_7(aq)$], solid Mn(III)-phthalocyanine chloride (Aldrich chemical), Mn(III)-acetyl acetonate (Aldrich), Mn(III)-tetra(4-pyridyl)porphine chloride (Aldrich), protein-bound Mn(III,IV) [oxygen-evolving complex of photosystem II (Riggs-Gelasco et al. 1996)], pyrolusite (β - MnO_2 , Aldrich), nsutite (γ - MnO_2 , Nsuta, Ghana), and synthetic todorokite [(Na,Ca,K)(Mg,Mn)Mn₂O₁₄·5H₂O]. The identity of all solid phases was verified by comparison to the JCPDS card file. Solids containing multiple phases were not used as models. Estimated standard deviations (ESDs) for fits to Mn K-edge data were obtained by analysis of transmission spectra measured from a series of well-defined mixtures of $MnSO_4$, Mn_2O_3 , and δ - MnO_2 (18 data points total), diluted and thoroughly homogenized into a low-absorbance $LiCO_3$ matrix. Linear-regression analyses of these references provided 1 σ error estimates: 1.7% for Mn(II), 2.6% for Mn(III), and 2.9% for Mn(IV). These values

TABLE 3. Results from first moment analysis and linear combination fits to emission spectra measured from SG-1 spores reacted with 10 μ M Mn(II)

Sample	1st moment less 6490 (eV) ± 0.01 eV	Fit A (%) $\pm 1\%$	Fit B (%) $\pm 1\%$	Fit C (%) $\pm 1\%$	Bulk Mn Oxidation State ± 0.02
MnCl ₂	0.97	100 / 0	100 / 0 (0)	100 / 0 / 0 (0)	2.00
0.22 d	0.41	30 / 70	31.0 / 69.0 (0.329)	29 / 9 / 62 (0.311)	3.18
0.45 d	0.33	20 / 80	20 / 80 (0.233)	18 / 9 / 73 (0.214)	3.37
0.85 d	0.25	9 / 91	10 / 90 (0.2835)	10 / -1 / 91 (0.283)	3.57
1.97 d	0.16	-2 / 102	-1 / 101 (0.317)	0 / -1.0 / 101 (0.317)	3.75
4.00 d	0.18	0 / 100	0 / 100 (0)	0 / 0 / 100 (0)	3.74*
Mn ₂ O ₃ (s)	0.40	-	-	-	3.00

Notes: Fit A = ratio of MnCl₂: 4.0 d sample components (expressed in %) determined using 1st moment. Fit B = ratio of MnCl₂: 4.0 d sample determined using two-component least-squares fit. Fit C = ratio of MnCl₂: Mn₂O₃: 4.0 d sample components determined using three-component least squares fits (see text). χ^2 values for least-squares fits are shown in parenthesis. Bulk Mn oxidation states (column 6) were calculated from fit C, assuming an oxidation state of 3.74 for the 4.0 d sample. Absolute accuracies are dominated by that for the 4.0 day sample.

* Absolute accuracy of this value is estimated at ± 0.09 (cf., methods section).

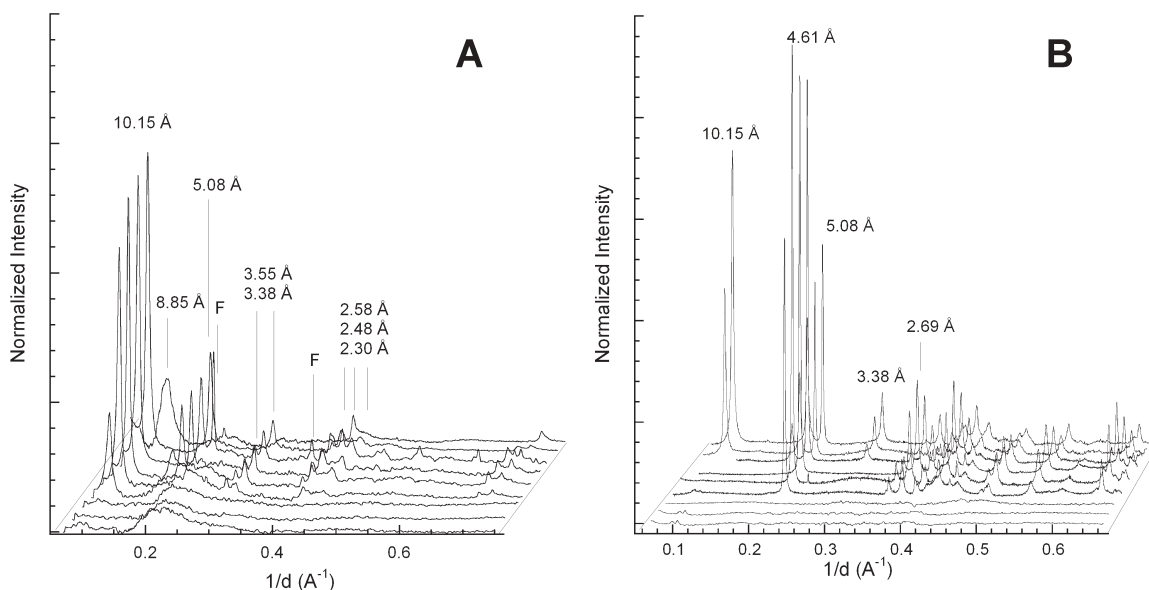


FIGURE 1. Synchrotron XRD intensity data for SG-1 spores reacted with Mn(II). (a) XRD data for 10 μ M Mn(II)-reacted samples. Reaction times from bottom to top are 0.22, 0.45, 0.85, 1.97, 4.0, 7.7, 12.7, 27.8, and 77 days. The first seven time points are transmission data, the last two are reflection geometry data. Broad, weak maxima at 0.2 to 0.25 \AA^{-1} are diffuse scattering from spores. "F" denotes feiknechtite peaks in the 12.7 d sample. (b) Reflection geometry XRD data from SG-1 spores reacted with 1 mM Mn(II) added once at start of reaction. Reaction times from bottom to top are 0.22, 0.45, 0.85, 1.97, 4.0, 7.7, 12.7, 27.8, and 77 days. The diffuse scattering from spores is removed from reflection XRD data during background removal of the large Kapton scattering peak.

are distinct from and substantially larger than the fit-derived ESDs (which typically had values of $\sim 0.5\%$). Thus, fit-derived ESDs are not reported.

RESULTS

Synchrotron radiation-based XRD measurements (SR-XRD)

X-ray diffraction intensity data from SG-1 spores reacted with 10 μ M Mn(II). Transmission SR-XRD intensity data for the 10 μ M Mn(II)-SG1 time series are shown in Figure 1A. The first three time points (6 through 22 h) show only broad, weak X-ray scattering peaks located between 0.2 and 0.25 \AA^{-1} , which arise from diffuse scattering from spores present in the samples. Samples reacted for 1.97 days and longer show well-defined Bragg peaks, the strongest three having d -spacings of 10.15, 5.08, and 3.38 \AA (Table 2). These diffraction lines correspond well to expected (001), (002), and (003) peak positions for 10 \AA phyllosulfates, which have structures similar to that of

birnessite (similar a and b unit-cell dimensions for the Mn octahedral layer) but contain a greater amount of structural water molecules in the interlayer (Burns and Burns 1977; Burns and Burns 1979; Kuma et al. 1994). The 10.15 \AA value agrees with the basal-plane spacing for a synthetic 10 \AA Na phyllosulfate reported by Kuma et al. (1994), but is larger than d -spacings reported for todorokite (~ 9.7 \AA) (Burns and Burns 1977). If the samples were allowed to dry in air at room temperature, then the putative 10 \AA phyllosulfate (001) peaks rapidly (within 30 minutes) decreased in size, indicating collapse of the 10 \AA structure as dehydration occurred (data not shown). This behavior indicates the importance of maintaining the samples in a hydrated state during measurement. Basal plane collapse is expected for hydrated phyllosulfates but not for todorokites. Therefore, we attribute the Bragg diffraction maxima observed at 10.15, 5.08, and 3.38 \AA , to a 10 \AA Na-bearing phyllosulfate and assign

them as (001), (002), and (003) reflections. The detection limit for this phase was estimated to be between 0.5 and 1% of the total dry mass of the solids, based on measurement of a series of physical mixtures of Na-birnessite and biogenic Mn oxides.

All samples, including the 0.22 d sample, were dark brown in color, due to the presence of Mn bio-oxides. Furthermore, as shown later in this manuscript, the XANES fitting results suggest that the primary bio-oxide is present at two to three times greater concentration than the 10 Å phyllosmanganate in the 1.97 d sample. From these observations, it can be inferred that the scattering intensity of the initial bio-oxide is substantially weaker than that of either the 10 Å phyllosmanganate or the diffuse scattering from the spores. Thus, we conclude that the initial bio-oxide is very poorly crystalline or X-ray amorphous.

There is an abrupt change in the XRD pattern of the 77 d sample. The 10 Å phyllosmanganate peaks are not present, having been replaced by a new set of broader, weaker reflections having a spacing of 8.85 Å. This change correlates with an overall decrease in the relative concentration of phyllosmanganate products, as measured by XANES. To our knowledge, an 8.85 Å *d*-spacing has not previously been reported for phyllosmanganates.

X-ray diffraction intensity data from SG-1 spores reacted with 1 mM Mn(II). Transmission SR-XRD intensity data for the 1 mM Mn(II)-SG1 time series are shown in Figure 1B and summarized in Table 2. The first three patterns [6 to 21 hours reaction with Mn(II)] show no well-defined X-ray scattering peaks, with the exception of a pair of peaks at about 0.1 Å⁻¹, barely discernable above the noise, which are observed in unreacted spores and therefore correspond to an unidentified cellular compound. The lack of diffuse scattering from the spores (between 0.2 and 0.25 Å⁻¹) reflects the lower sensitivity of the reflection geometry technique to distinguish peaks in the region where water scattering is significant (0.2 to 0.5 Å⁻¹), as compared to transmission geometry. Samples reacted for 1.97 days and longer show well-defined Bragg peaks, which correspond to feitknechtite, β-MnOOH (JCPDS card file 18-0804). The detection limit for feitknechtite was estimated to be between 0.5 and 1% of the total dry mass of the solids, based on measurement of a series of physical mixtures of a α-MnOOH and biogenic oxides. The last two patterns (27.8 and 77 days of reaction) show a decrease in the relative heights of the feitknechtite peaks, and the emergence of peaks corresponding to a 10 Å phyllosmanganate. This decrease correlates with a drop in the concentration of aqueous Mn(II) (Table 1).

SR-based $K\beta_{1,3}$ XES measurements of SG-1 spores reacted with 10 μM Mn(II)

It is known that Mn *K*-edge XANES are affected by Mn oxidation state as well as by the ligand type (Visser et al. 2001). In contrast, $K\beta_{1,3}$ XES has been shown to be a more direct probe of Mn oxidation state and is less sensitive to ligand identity (Bergmann et al. 1998; Messinger et al. 2001; Visser et al. 1992). XES can therefore provide an independent bulk-scale in situ probe of Mn oxidation state in complex cell/biooxide mixtures. $K\beta$ emission arises from the 3p → 1s transition, which is sensitive to the number of unpaired 3d electrons of the fluorescing atom (Peng et al. 1994; Tsutsumi et al. 1976; Urch and Wood 1978). In the case of high-spin Mn systems [including all relevant Mn

oxides and bacterial intracellular Mn(II)], the number of unpaired 3d electrons relates directly to the oxidation state, going from 5 unpaired electrons in the case of Mn(II) down to zero in the case of Mn(VII) (Bergmann et al. 1998; Messinger et al. 2001; Visser et al. 1992). When the oxidation state of Mn increases from Mn(II) to Mn(IV), fewer unpaired 3d valence electrons are available to interact with the 3p hole, and the magnitude of the 3p-3d exchange interaction becomes smaller. This leads to a decrease in the $K\beta'$ – $K\beta_{1,3}$ splitting (Taguchi et al. 1997), hence the $K\beta_{1,3}$ emission peak shifts to lower energy as Mn is oxidized. $K\beta_{1,3}$ spectra from reference Mn(II), Mn(III), and Mn(IV) compounds are shown at the bottom of Figure 2. As the Mn oxidation state increases, the peak shifts down in energy by about 0.5 eV for each successively higher oxidation state.

In this study, XES analysis focused on short reaction times where Mn(III) intermediates (if present) would be most prominent as a fraction of total Mn. Accordingly, 10 μM Mn(II) incubation time points up to 4 days were selected for analysis. The 1 mM incubation samples were not analyzed by XES because of the presence of interfering Mn(III) secondary reaction products (as detected by XRD and XANES). Results are shown in the top of Figure 2 (spectra from 0.85 and 1.97 day samples would overlay on top of the 4.0 day sample and are omitted for clarity). Energy shifts in the $K\beta_{1,3}$ emission were quantified using a 1st-moment analysis (Messinger et al. 2001; Visser et al. 2001), which provides an accuracy of ~0.01 eV for energy shifts (Table 3). The first moment of the spore samples shifts smoothly downward from 0.22 d through 1.97 d reaction time, indicating a steady progression of Mn oxidation states to higher values

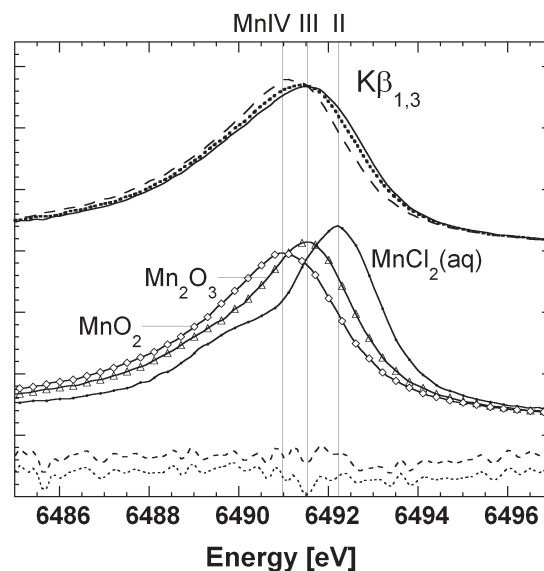


FIGURE 2. Top: $K\beta$ emission spectra of SG-1 spores reacted with 10 μM Mn(II) for 0.22 (solid line), 0.45 (dotted line), and 4.0 days (dashed line). (Spectra from 0.85 and 1.97 day samples would overlay on top of the 4.0 day sample and are omitted for clarity). Middle: Mn reference compounds MnCl₂(aq), Mn₂O₃, and β-MnO₂ (pyrolusite). Spectra are normalized to the integrated peak intensity. Bottom: dashed line is the residual from the two-component (MnII + IV) fit to the 0.22 d $K\beta$ emission spectrum; dotted line is the residual for the three-component (MnII + III + IV) fit to the 0.22 d spectrum. See text for details.

through this period. Between 1.97 and 4.0 d reaction, there is a very slight upward shift of the moment energy, indicating that the oxidation state of the 4.0 day sample is slightly lower than that of the 1.97 day sample.

The XES spectrum from the 4.0 d sample was fit with linear combinations of emission spectra from MnCl_2 , Mn_2O_3 , and $\delta\text{-MnO}_2$ (Mn oxidation state of 3.84) reference compounds to determine a bulk Mn oxidation state of +3.74. This sample was then used as an end-member component in two-component [Mn(II) and the biooxide component] least-squares linear combination fits to the remaining incubation samples. Results are summarized in Table 3 ("Fit B"). Also shown in Table 3 are the results of two-component compositional analyses ("Fit A") using the first moments from the sample spectra (cf., methods section). The first moment analyses agree closely with the two-component linear combination fits, and both show the progression of bulk Mn oxidation state from 3.18 to 3.74 (Table 3) as reaction time increases from 0.25 to 4.0 d. To test for the presence of a separate Mn(III) phase, three-component least-squares, linear combination fits were performed using either Mn_2O_3 or MnOOH in addition to the other two components. Mn_2O_3 produced the best fits, and the corresponding results are shown in Table 3 ("Fit C"). Addition of Mn(III) to the fits as a third component does not significantly improve the fit quality relative to the two-component fits. This is illustrated in the bottom of Figure 2, which shows difference spectra of the two-component and three-component fits to the 0.22 d. spectrum. These results indicate that the samples are dominated by two components—Mn(II) and the bio-oxides—and suggests that a separate Mn(III) species is not present above detection limit ($\sim 10\%$ of total Mn).

Mn K-edge XANES measurements

XANES spectra of SG-1 spores reacted with 10 μM Mn(II). Manganese K-edge XANES spectra for the 10 μM Mn(II)-reacted SG-1 spore samples as a function of time (5.25 hours to 77 days) are shown in Figure 3. Fits were attempted using spectra from a number of Mn oxides, including $\delta\text{-MnO}_2$,

pyrolusite, nsutite, todorokite, several birnessites, and α -, β -, and γ - MnOOH . It was found that excellent reproductions of the initial 10 μM -reacted SG-1 sample spectra could be obtained using linear combinations of three component spectra: intracellular Mn(II) (measured from clean, unreacted SG-1 spores), $\delta\text{-MnO}_2$, and Mn(II) adsorbed on spores in excess of intracellular Mn. The latter (minor) component was added because it is expected to be present, and its XANES spectrum is distinct from that of intracellular Mn(II). The same overall fit result was reported for oxidation of 100 μM Mn(II) by SG-1 spores over the time period 0 to 9 hours (Bargar et al. 2000). The fit decomposition for the 0.22 d time point is shown in Figure 3. This spectrum has a pronounced shoulder at 6553 eV, mostly due to the presence of intracellular Mn(II). This feature is followed at slightly higher energy by the absorbance maximum, at 6562 eV. This position and the shape of the absorbance maximum are described best by that of $\delta\text{-MnO}_2$ (oxidation state 3.84 ± 0.06). Hexagonal birnessite has an edge shape and energy position generally similar to that of $\delta\text{-MnO}_2$ (Villalobos et al. 2003). However, the specific height and width of the $\delta\text{-MnO}_2$ absorbance maximum differ from those of our hexagonal birnessite spectra, and the former spectrum consistently provided significantly better fits (chi-squared residual lower by a factor of ≥ 2) to the experimental data.

The energy position of the XANES absorbance maximum increases with increasing oxidation state, due to a decrease in charge screening the 1s electron from the positive charge of the Mn nucleus. In evidence of this behavior, the absorbance maxima for $\text{Mn}^{2+}(\text{aq})$, $\beta\text{-MnOOH}$, $\alpha\text{-MnOOH}$, triclinic birnessite (oxidation state 3.57), and $\delta\text{-MnO}_2$ (oxidation state 3.84) increase in the order (in eV): $6553 < 6559.2 < 6560.5 < 6561.2 < 6562.1$. XANES absorbance maxima energy positions of 6561.9 to 6562.1 eV are obtained for $\delta\text{-MnO}_2$ and for acid birnessites having oxidation states between 3.70 and 3.90 (Villalobos et al. 2003). Comparison of this result to the sample spectra suggests that the Mn oxidation state of the initial biooxide product lies between 3.70 and 4.0, in agreement with the XES results.

The proportion of intracellular Mn(II) decreases with increas-

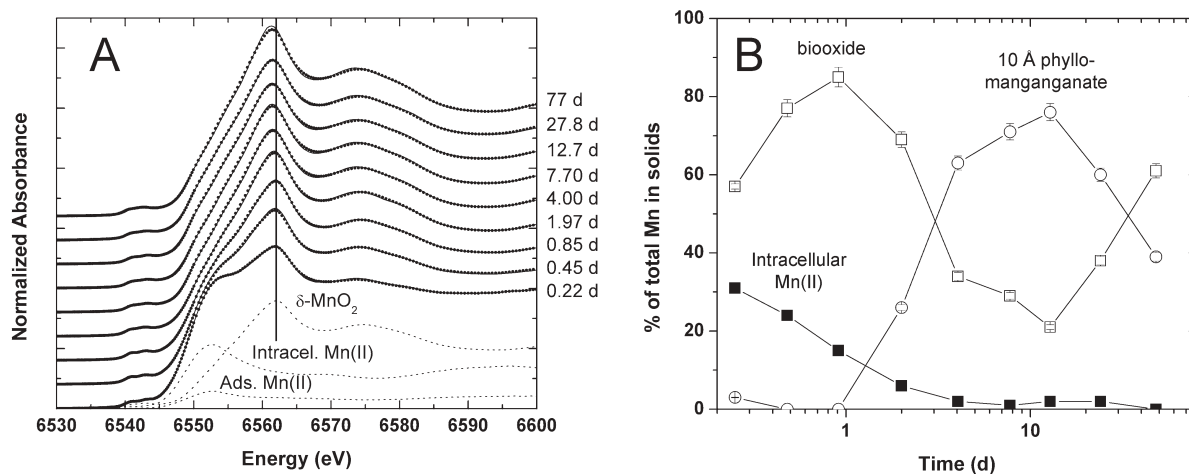


FIGURE 3. (a) Manganese K-edge XANES spectra (solid lines) of SG-1 spores reacted with 10 μM Mn(II). Heavy dotted lines are fits to spectra (c.f., Table 2). The fit deconvolution (light dotted lines) is presented for the 0.22 d sample. Vertical line at 6562 eV marks the energy position of the absorbance maximum for the biooxide. (b) Summary of XANES fit results. Fit components: intracellular Mn(II) (solid squares), biooxide (open squares), and 10 \AA phyllo-manganate (open circles). Error bars are shown that, in some cases, are smaller than the markers.

ing reaction time, consistent with accumulation of biogenic oxides in the samples. Beginning at a reaction time of 1.97 days, after adding a second 10 μM aliquot, and continuing until 27.8 days, the energy position of the absorbance maximum starts to shift down from 6562 eV and eventually obtains a value of 6561.4 eV. Aside from this energy shift, there is little change in the shapes of the XANES spectra. This behavior suggests a slight decrease in the average oxidation state of solid-phase Mn (also observed in XES measurements), such as could occur if a second solid phase with a Mn local structure similar to that of $\delta\text{-MnO}_2$ were to form. The onset of this behavior coincides with the shift to a slightly lower Mn oxidation state observed in the XES results and to the appearance and growth of a crystalline 10 \AA phylломanganate in the XRD results. To account for this behavior (i.e., red shift of XANES maximum and presence of phylломanganate), an additional phylломanganate component was added to the XANES fits. Excellent fit reproductions were obtained when a triclinic Na birnessite component, for which the average Mn oxidation state was 3.57 (Villalobos et al. 2003), was added to the fits. These trends are summarized graphically in Figure 3, which shows the initial rapid production of the primary biooxide, followed by production of the 10 \AA phylломanganate.

Following 12.7 days of reaction, the trend toward apparently increasing Mn(III) content reversed, and the edge shifted back toward higher energy values for the absorbance maximum and a higher apparent content of the $\delta\text{-MnO}_2$ -like biooxide. This change follows a substantial drop in aqueous Mn(II) concentration in the experiment, from 3.38 μM at 4 days to 140 nM at 12.7 d. This behavior suggests that Mn(II) can act as a reductant in the system (i.e., lowering the apparent oxidation state of the bio-oxides between 0.85 and 12.7 days reaction time), and its disappearance is followed by a rebound in the oxidation state of the bio-oxides.

XANES spectra of SG-1 spores reacted with 1 mM Mn(II).

Two sets of incubation experiments were performed at 1 mM Mn(II) concentration; in one, a single addition of Mn(II) was

made at the beginning of the experiment to obtain 1 mM. The Mn(II) concentration was subsequently allowed to decrease to sub- μM concentrations as the oxidation reaction proceeded. This procedure was chosen initially to facilitate comparison to the prior study of Mn(II) oxidation by SG-1 spores by Mandernack et al. (1995). This sample series was reacted for up to 77 d in parallel with the 10 μM experiment. Feitknechtite ($\beta\text{-MnOOH}$) is stable relative to MnO_2 at Mn(II) concentrations greater than about 0.5 mM under the experimental conditions (Mandernack et al. 1995). In acknowledgement of this thermodynamic threshold, a second series of 1 mM Mn(II) incubations was performed in which the Mn(II) concentration was maintained between 0.68 and 0.96 mM (Table 1). This latter experimental series was terminated after 9 days because reaction products appeared to have obtained a stable mineralogy (feitknechtite) as soon as 1.97 d reaction, showing no changes between 4 and 9 days.

The XANES spectra from the single-addition 1 mM Mn(II) incubation are provided in Figure 4. The corresponding fitting results are summarized in Figure 4 and Table 4. During the initial time points (up to 6 hours reaction), the 1 mM results are similar to the results obtained at 10 μM Mn(II). The initial solid product is a $\delta\text{-MnO}_2$ -like phase, which reaches a concentration of about 51% of total solid Mn within 6 hours of reaction. Thereafter, feitknechtite ($\beta\text{-MnOOH}$) is rapidly produced, reaching nearly 100% of the Mn after 1.97 days of reaction. After 12.7 days reaction, the amount of feitknechtite decreased dramatically. The same results were obtained in the XRD measurements. The decrease in feitknechtite concentration correlates with a drop in the concentration of aqueous Mn(II) to sub-micromolar levels (Table 1), suggesting thermodynamic control over its stability. The results from the 1mM maintained-Mn(II)-concentration incubation series are summarized in Table 4 and compared to an abiotic control experiment in Figure 5. Again, a $\delta\text{-MnO}_2$ -like biooxide was quickly produced, but feitknechtite quickly became the dominant form and remained thus throughout 9 days of reaction (Table 4).

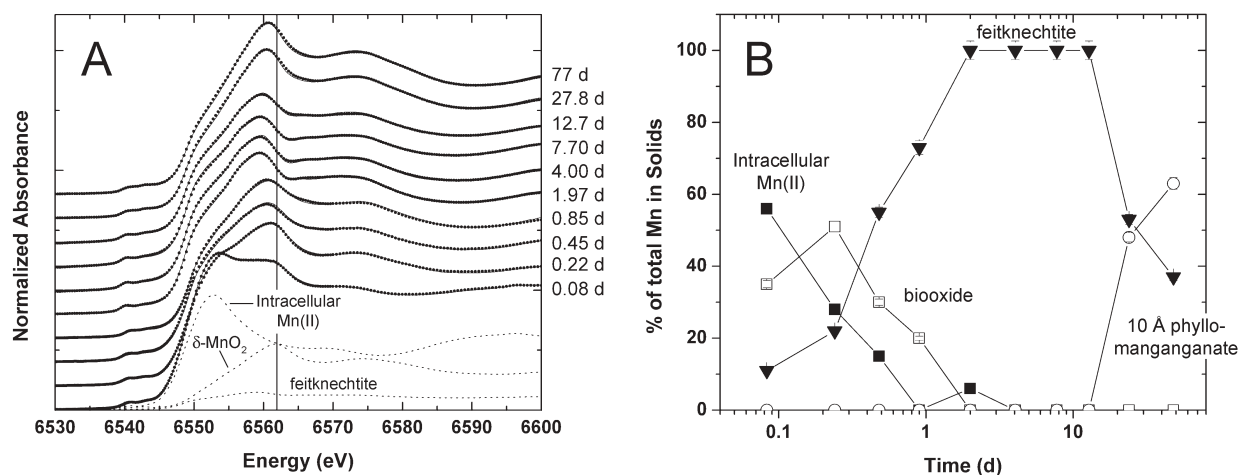


FIGURE 4. (a) Manganese *K*-edge XANES spectra (solid lines) of SG-1 spores reacted with 1 mM Mn(II). Heavy dotted lines are fits to spectra (cf. Table 2). The fit deconvolution (light dotted lines) is presented for the 2 hour sample. Vertical line at 6562 eV marks the energy position of the absorbance maximum for the biooxide. (b) Summary of XANES fit results. Fit components: intracellular Mn(II) (solid squares), biooxide (open squares), feitknechtite (solid triangles), and 10 \AA phylломanganate (open circles). Error bars are shown that, in some cases, are smaller than the markers.

TABLE 4. Linear combination fits to Mn K-edge XANES spectra, expressed in mole % of total manganese present

10 μM Mn(II)											
Reaction Time (d):			0.22	0.45	0.85	1.97	4.00	7.70	12.7	27.8	77.0
Fluo / Trans*	–	–	Fl	Tr	Tr	Tr	Tr	Tr	Tr	Tr	Tr
Adsorbed Mn(II)	–	–	9	–	–	–	–	–	–	–	–
Spore Mn(II)	–	–	31	24	15	6	2	1	2	2	–
$\delta\text{-MnO}_2$	–	–	57	77	85	69	34	29	21	38	61
Na Birnessite	–	–	3	0	0	26	63	71	76	60	39
1 mM Mn(II), single addition at start											
Reaction Time (d):		.083	0.22	0.45	0.85	1.97	4.00	7.70	12.7	27.8	77.0
Fluo / Trans	–	Fl	Tr	Fl	Tr	Fl	Fl	Fl	Fl	Fl	Fl
Spore Mn(II)	–	56	28	15	6	–	–	–	–	–	–
$\delta\text{-MnO}_2$	–	35	51	30	20	–	–	–	–	–	–
Feitknechtite	–	11	22	55	73	100	100	100	100	53	37
Na Birnessite	–	–	–	–	–	–	–	–	–	48	63
1 mM Mn(II), maintained throughout experiment by repeated additions											
Reaction Time (d):	.041	0.13	0.25	0.5	0.96	2.00	4.00	9.00	–	–	–
Fluo / Trans	Tr	Tr	Tr	Tr	Tr	Tr	Tr	Fl	–	–	–
Spore Mn(II)	24	21	14	4	2	–	–	–	–	–	–
$\delta\text{-MnO}_2$	71	68	63	18	20	5	2	–	–	–	–
Feitknechtite	6	12	24	78	79	95	97	100	–	–	–
Na Birnessite	–	–	–	–	–	–	–	–	–	–	–
Abiotic Control: 100 μM Mn(II) + $\delta\text{-MnO}_2$											
Reaction Time (d):	0	–	–	0.5	0.90	–	–	–	–	–	–
Fluo / Trans	Tr	–	–	Fl	Fl	–	–	–	–	–	–
Mn(II)	0	–	–	11	8	–	–	–	–	–	–
$\delta\text{-MnO}_2$	100	–	–	59	54	–	–	–	–	–	–
Na Birnessite	0	–	–	30	37	–	–	–	–	–	–
Abiotic Control: 1 mM Mn(II) + $\delta\text{-MnO}_2$											
Reaction Time (d):	0	.11	0.14	0.21	0.28	0.94	1.99	2.23	–	–	–
Fluo / Trans	Fl	Fl	Fl	Fl	Fl	Fl	Fl	Fl	–	–	–
Mn(II)	2	2	2	1	–	–	–	–	–	–	–
$\delta\text{-MnO}_2$	98	56	42	40	33	24	16	7	–	–	–
Feitknechtite	–	41	56	58	67	76	84	93	–	–	–

Note: ESDs for fit values are $\pm 1.7\%$ for Mn(II), $\pm 2.6\%$ for Mn(III), and $\pm 2.9\%$ for Mn(IV) (cf., section 2.2).

* Fl = fluorescence; Tr = transmission.

Abiotic control experiments: reaction of 10 μM and 1 μM Mn(II) with $\delta\text{-MnO}_2$

A 10 Å phyllomanganate phase and feitknechtite are observed in the biogenic oxide samples only after substantial amounts of the $\delta\text{-MnO}_2$ -like biooxide are created, leading one to question whether the 10 Å phyllomanganate and feitknechtite are secondary reaction products. A series of experiments was performed to test the hypothesis that Mn(II) could react with fresh $\delta\text{-MnO}_2$ to produce these phases as observed in the presence of SG-1 spores. The results obtained in 100 μM Mn(II) are shown in Figure 6 and Table 4. Under these conditions, ~ 0.5 eV downshift of the XANES absorbance maximum was observed and a phyllomanganate (as assigned by fit using triclinic birnessite) was formed. This solid reached 37% of total Mn within 21.5 hr reaction time. The results of abiotic reaction of $\delta\text{-MnO}_2$ with a 1 mM Mn(II) solution are presented in Figure 5 and Table 4. As can be seen, feitknechtite is produced rapidly, at rates similar to those observed in the maintained 1 mM Mn(II) / SG-1 spore incubations.

DISCUSSION

Primary solid products of Mn(II) oxidation by SG-1 spores

SR-XRD and XANES measurements indicate the initial solid products in the incubation experiments to be X-ray amorphous oxides resembling $\delta\text{-MnO}_2$. This initial biooxide is the only solid phase observed during the first day of reaction at 10 μM Mn(II) and is the dominant product observed within the first 0.22 days of reaction at 1 mM Mn(II). These results are consistent with previous XANES measurements of 100 μM Mn(II) oxidation by

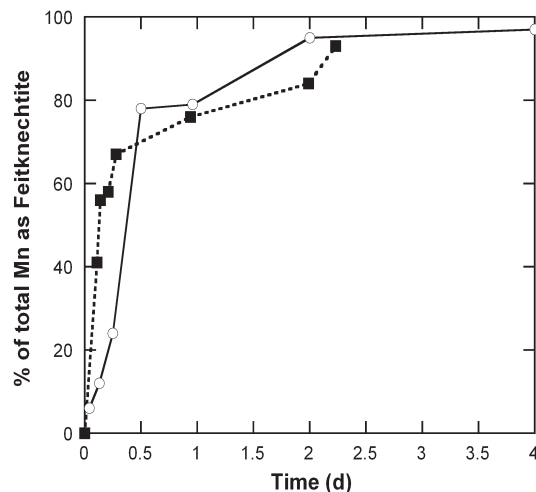


FIGURE 5. Feitknechtite evolution as a function of time when SG-1 spores are reacted with Mn(II) maintained between 0.68 and 1 mM (open circles). Solid squares give results obtained when 1 mM Mn(II) is reacted with $\delta\text{-MnO}_2$ in the absence of spores.

SG-1 spores conducted from 0 to 9 hours of reaction (Bargar et al. 2000). XANES and XES measurements in the present study indicate the Mn oxidation state in the biooxide to be between 3.7 and 4.0.

$\delta\text{-MnO}_2$ is believed to be a disordered hexagonal phyllomanganate containing Mn(IV) vacancy defects, having very small particle size (<100 nm lateral dimensions), and having only two

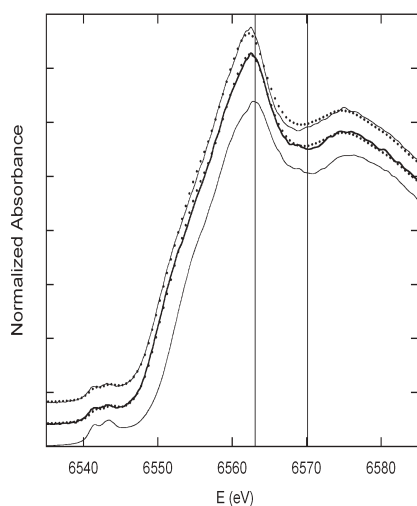


FIGURE 6. Manganese *K*-edge XANES spectra (solid lines) of δ - MnO_2 reacted with $100 \mu\text{M}$ Mn(II) in the absence of SG-1 spores. Dotted lines are fits to spectra (cf., Table 2). Reaction times from bottom to top are 0 h (parent δ - MnO_2 material), 12, and 21.5 h. The vertical line at about 6562 eV marks the energy position of the absorbance maximum for the δ - MnO_2 component. The vertical line at 6570.5 eV marks the energy position first XANES minimum for the δ - MnO_2 component. Both features shift to lower energy with reaction progression.

or three MnO_2 layers (Mn is in octahedral coordination) stacked along the *c* axis (Villalobos et al. 2003). The small number of stacked layers causes the (00*l*) reflections to become broad and weak or to be completely absent. Successive MnO_2 layers are believed to be pseudo-randomly sheared in the *a*-*b* plane and rotated relative to one-another along the *c* axis (i.e., turbostratic disorder), which destroys the coherence required to generate well-defined (*hkl*) reflections (Chukhrov et al. 1987; Lanson et al. 2000; Reynolds 1989; Villalobos et al. 2003). The resulting (*hk*) reflections are weak, broad, and asymmetric. If the particles are sufficiently small and disordered, then their diffracted intensities may be too weak to detect above background (Reynolds 1989), resulting in an X-ray amorphous material.

Consideration of these points leads to a structural model for the initial bio-oxides observed in this study. SG-1 spores are believed to oxidize Mn(III) to (IV) via an enzymatic pathway (Webb et al. 2004). The subsequent release of Mn(IV) should be followed immediately by hydrolysis and polymerization of Mn(IV), due to its low solubility in water (Baes and Mesmer 1976). Based on the present results, it is reasonable to propose that Mn(IV) polymerization leads to sheet polymers or nanoparticles with general structural formula $\text{Mn}_x\text{O}_2^{(4x-4)}$ ($x \leq 1$) that exhibit the basic hexagonal phyllosilicate topology, but contain numerous vacancy defects (i.e., $x < 1$) and other structural defects such as Mn(II) or Mn(III) bonded above vacancy sites in the hexagonal sheets as a result of reaction with aqueous Mn(II) (Fig. 7). In support of this model, Bargar et al. (2004) reported that bio-oxides formed in seawater by SG-1 spores exhibited disordered hexagonal phyllosilicate structures, and this general result also was reported for Mn bio-oxides produced by *P. putida* (Villalobos et al. 2003). The sheet polymer model proposed for the initial bio-oxides in the present study assumes the hexagonal $\text{Mn}_x\text{O}_2^{(4x-4)}$ sheets to have nanoparticulate lateral

dimensions (e.g., < 20 nm) and little or no stacking normal to the layers, and therefore to be X-ray amorphous as measured in this study.

Secondary product transformations following Mn(II) oxidation by SG-1 spores

After 1.97 days of reaction with $10 \mu\text{M}$ Mn(II) , a crystalline 10 \AA phyllosilicate was observed by SR-XRD and XANES in the spore samples (Figs. 1 and 3; Tables 2 and 4). Abiotic reaction of Mn(II) with δ - MnO_2 suggests that a phyllosilicate phase similar to that observed in the spore incubations can be obtained following abiotic reaction of Mn(II) with δ - MnO_2 (Fig. 6). Based on this result, and on the observation that production of the 10 \AA phyllosilicate lags behind that of the δ - MnO_2 -like biogenic oxide, we interpret the 10 \AA phyllosilicate phase to be an abiotic, secondary reaction product, produced by reaction of Mn(II) with the primary biogenic oxide. In the presence of 1 mM Mn(II) , feitknechtite (β - MnOOH) is rapidly produced in spore incubation experiments (Figs. 4 and 5). The rate of feitknechtite production in abiotic control experiments was found to be similar to the maintained 1 mM $[\text{Mn(II)}]$ spore incubations (Fig. 5). Therefore, feitknechtite production also can be attributed to abiotic reaction of Mn(II) with the primary biogenic oxide. This general reaction pathway is illustrated schematically in Figure 7.

The latter conclusion is strengthened by equilibrium thermodynamics arguments. Thermodynamic stability relationships in the Mn(II)/(III)/(IV) system were reviewed by Mandernack et al. (1995), and can be summarized as follows: the stability of Mn(III)-bearing phases such as MnOOH and Mn_3O_4 increases relative to that of Mn(IV)-bearing phases such as MnO_2 as pH and Mn(II) concentration increase. This behavior can be appreciated from inspection of the reaction for MnOOH transformation to MnO_2 in aqueous solution:



Mass action will cause this reaction to move toward the left-hand side of the equation when the activities of Mn^{2+} or OH^- increase. The point at which MnOOH and MnO_2 are in equilibrium is described by a line in pH- $[\text{Mn(II)}]$ space, the location of which depends upon the free energies of the MnOOH polymorph and MnO_2 phases being compared. If feitknechtite and sodium birnessite are chosen for comparison at 25°C and pH = 7.8 (HEPES buffer), then equilibrium between these phases is predicted to occur at a Mn^{2+} concentration ($[\text{Mn}^{2+}(\text{aq})]$) of about 0.5 mM (Mandernack et al. 1995). Accordingly, if feitknechtite is produced as a result of any reaction, then it will be stable with respect to transformation to birnessite so long as $[\text{Mn}^{2+}(\text{aq})] > 0.5 \text{ mM}$. Conversely, if $[\text{Mn}^{2+}(\text{aq})]$ drops below this equilibrium balance point, then the transformation of feitknechtite to birnessite will be energetically favored and may proceed if a reaction pathway exists. It is important to note that these equilibrium relations do not forbid the formation of feitknechtite or other Mn(III)-bearing oxides at $[\text{Mn}^{2+}(\text{aq})] < 0.5 \text{ mM}$. Such phases can be produced any time that a reaction pathway and driving force exist and kinetics are favorable. The analysis above applies only to the equilibrium between Mn(III)-bearing phases and MnO_2 .

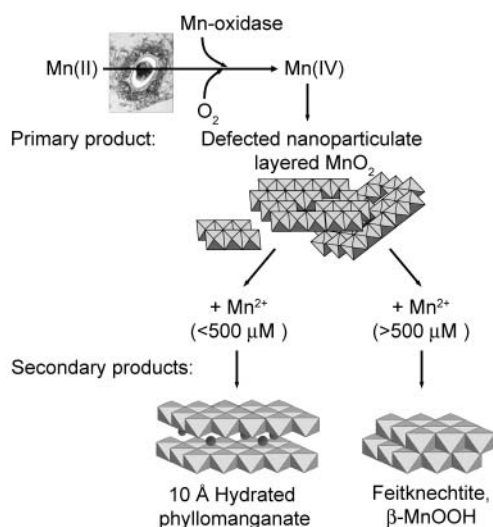


FIGURE 7. Schematic representation of proposed reaction sequence for biogenic Mn oxides and secondary reaction products. Enzymatic oxidation step depicted at beginning of reaction is based on Webb et al. (2004) and Tebo et al. (2004).

The occurrence of feitknechtite in the spore incubations and in the abiotic control experiments is consistent with an abiotic thermodynamic reaction mechanism. Feitknechtite was not observed in any of the samples prepared at 10 μM initial [Mn²⁺(aq)] in this study {[Mn²⁺(aq)] is approximately equivalent to [Mn(II)]_i under the experimental conditions of the present study (Baes and Mesmer 1976)}, with the single exception of trace amounts detected by XRD in the 12.7 d 10 μM incubation. In contrast, feitknechtite was produced in all samples prepared at 1 mM initial [Mn²⁺(aq)]. This behavior suggests that feitknechtite is generated only when it is stable with respect to disproportionation to MnO₂.

In the 10 μM incubation and one of the 1 mM incubations, [Mn²⁺(aq)] fell during the reaction. In both cases, this drop was followed by changes in the mineralogy of the samples. In the 10 μM incubation, a decrease in [Mn²⁺(aq)] below 10 nM (after 12.7 days) was followed by an apparent increase in the oxidation state of the dominant oxides, a twofold decrease in the concentration of the 10 Å Na phylломanganate, and the appearance of a new, poorly crystalline phase with an 8.85 Å *d*-spacing. Thus, the stability of the 10 Å Na phylломanganate secondary product appears to be controlled by the Mn(II) concentration. In the 1 mM incubation, falling [Mn²⁺(aq)] was followed after 12.7 days of reaction by a reduction in the feitknechtite concentration from 100% to 37%. Again, this observation suggests that the stability of the secondary products is controlled by the Mn(II) concentration present in the experiments.

Constraints on bacterial oxidation mechanisms

No evidence was observed for the existence of Mn(III) species or solid phases intermediate to the production of the primary biogenic oxide under the bulk conditions of this study. Thus it can be concluded that, should Mn(III) intermediates have existed in our samples, they occurred below the detection limits for these techniques, which is >5% of total Mn. Such a conclusion is consistent with reports that the enzymatic Mn(III) → Mn(IV)

oxidation step is significantly faster than the Mn(II) → Mn(III) step as catalyzed by SG-1 spores (Webb et al. 2004). Therefore, Mn(III) intermediates should be consumed more rapidly than they are produced and should be present in the samples only at small concentrations. Hastings and Emerson (1986) suggested that hausmannite (Mn₃O₄) occurred as an intermediate in the oxidation of Mn(II) by spores of SG-1 spores. Our results do not corroborate this hypothesis. Furthermore, as discussed by Mandernack et al. (1995), hausmannite, α-MnOOH, and γ-MnOOH, are stable with respect to transformation to MnO₂ (Reaction 1 above) when [Mn²⁺(aq)] is greater than 5 × 10⁻⁷ M (at pH = 7.8). [Mn²⁺(aq)] was well in excess of this threshold during the initial periods of our experiments, and we therefore do not expect these solid phases to occur as intermediates (if they did, they would be stable products).

Comparison to previous studies: occurrence of Mn(III) and Mn(II,III) (oxyhydr-)oxides

Mandernack et al. (1995) studied Mn(II) oxidation products of *Bacillus* sp., strain SG-1 after two-week incubations performed over a range of [Mn(II)], temperature, and ionic strength conditions. For room-temperature HEPES-buffered incubations, they reported that at increasing initial Mn(II) concentrations, solids of increasing crystallinity and decreasing oxidation state occurred. At 10 μM initial [Mn²⁺(aq)], a poorly crystalline, unidentifiable Mn oxide was observed. At higher initial [Mn²⁺(aq)], the following products were identified: a 10 Å phylломanganate (100 μM), feitknechtite + manganite (γ-MnOOH) (1 mM), and manganite + hausmannite (10 mM). Based on the thermodynamics discussed above and analogy with our present results, we interpret the feitknechtite, manganite, and hausmannite observed in this previous study as being abiotic secondary reaction products. Hastings and Emerson (1986) used TEM to study the products of the SG-1 reaction with Mn(II) added at concentrations of 2 μM. They reported the dominant Mn oxidation product to be an amorphous nanoparticulate solid with a crumpled sheet-like texture. This material likely corresponds to the biogenic δ-MnO₂-like product identified in the current work. Scanning transmission X-ray microscopy measurements (~100 nm spatial resolution) of SG-1 spores reacted with 10 mM Mn(II) (5 day reaction at pH = 7.5) indicated the association of abundant Mn(III) (up to 62% of the total Mn) with spore cells (Pecher et al. 2003). The speciation of the Mn(III) could not be determined in this previous study. Only small concentrations (<20%) of Mn(IV) were found to occur. Based on the results of the current study, the presence of Mn(III) and relative lack of MnO₂ can be attributed to feitknechtite precipitation. Mann et al. (1988) reported that hausmannite was produced by SG-1 spores reacted with 25 mM Mn(II) at pH = 7.5. This product can be attributed to abiotic reaction of Mn(II) with biogenic oxides. Greene and Madgwick (1991) reported that an Mn(II)-oxidizing *Pseudomonas* species produced manganite and then γ-MnO₂ following reaction with 91 mM Mn(II). Again, we speculate that these oxides were abiotic products, formed via reaction of Mn(II) with a primary poorly crystalline phase. In a few instances, trace quantities of crystalline oxides were observed following biogenic oxidation at low Mn(II) concentrations (<10 μM). The occurrence of extreme trace amounts of hausmannite in the Hastings and Emerson (1986) study can be

attributed to abiotic reaction of Mn(II) with the poorly crystalline biogenic oxide because the $[Mn^{2+}(aq)]$ used in that experiment exceeded the thermodynamic threshold of $\sim 10^{-7} M$ required for MnO_2 transformation to hausmannite. The occurrence of trace amounts of feitknechtite at $10 \mu M [Mn^{2+}(aq)]$ in the present study (12.7 d sample) cannot be attributed easily to abiotic oxidation of Mn(II) because of the low value of $[Mn^{2+}(aq)]$ relative to the feitknechtite/ MnO_2 threshold. It is therefore attributed to direct precipitation of feitknechtite, which is a favored abiotic pathway (Hem and Lind 1983) but is very slow in comparison to bacterial catalysis. This process is presumed to occur in parallel (but at a much slower rate than) with the bacterial pathway.

Implications for environmental occurrences of Mn bio-oxides and secondary products

Untransformed primary Mn bio-oxides may be abundant in settings in which Mn(II) is scarce (less than $\sim 1 \mu M$), such as in the oxic water column of open seas and lakes. However, Mn(II) often occurs at concentrations higher than this in natural waters, and frequently exhibits significant concentration variations during seasonal and daily cycles (Hem 1989; Warren and Haack 2004). Spatial gradients in Mn(II) concentration are also common. Manganese oxides settling through suboxic and anoxic water columns and near point sources such as hydrothermal vents will experience significant changes in $[Mn(II)]$. Acid mine drainage impacted areas may have advancing fronts with high Mn concentrations (Fuller and Harvey 2000). Remediation of such contaminant sources will be followed by long-term decreases in Mn(II). Based on the results of this study, it is likely that abiotic mineralogical transformations are commonplace in such settings, and that abiotic secondary Mn oxides will be volumetrically important following bacterial Mn(II) oxidation when dissolved Mn(II) is abundant. Such mineralogical transformations may pose redox conditions around bacterial cells, liberate sorbed metal ions, or alter the rates of surface-mediated processes that control the activities of dissolved species. It is plausible that microbes may exploit such reactions to indirectly buffer or otherwise control specific chemical conditions in the vicinity of the cell.

In cases where it is desirable to study a primary biogenic Mn oxide, careful consideration of the desired reaction conditions and close monitoring of phase evolution over appropriate time scales will be required in order to avoid undesired reaction products.

ACKNOWLEDGMENTS

We thank Anna Obratsova for spore preparations, Apurva Mehta for his assistance with SR-XRD measurements, and Joe Rogers for his help with instrument design. We thank Alan Stone for providing synthetic manganite and Jim Penner-Hahn for providing the spectrum for photosystem II. This work was supported by the NSF grants to BMT/JRB (EAR-9725845 and CHE-0089208) and BMT (MCB-9808915). We thank B.L. Cox for assistance with XES measurements. SSRL and APS are national user facilities operated on behalf of the U.S. DOE, Office of Basic Energy Sciences. The SSRL SMB Program is supported by the DOE, Office of Biological and Environmental Research, and by the NIH National Center for Research Resources, Biomedical Technology Program. APS-BioCAT is supported by NIH under contract RR-08630.

REFERENCES CITED

- Baes, C.F. and Mesmer, R.E. (1976) *The Hydrolysis of Cations*. Wiley, New York.
- Bargar, J.R., Tebo, B.M., and Villinski, J.E. (2000) In situ characterization of Mn(II) oxidation by spores of the marine *Bacillus* sp. strain SG-1. *Geochimica et Cosmochimica Acta*, 64, 2737–2749.
- Bargar, J.R., Webb, S.M., and Tebo, B.M. (2005) EXAFS, XANES, and in-situ SR-XRD characterization of biogenic manganese oxides produced in sea water. *Physica Scripta*, in press.
- Bergmann, U. and Cramer, S.P. (1998) A high-resolution large-acceptance analyzer for X-ray fluorescence and raman spectroscopy. *Proceedings of SPIE*, 3448, p. 198–209.
- Bergmann, U., Grush, M.M., Horne, C.R., DeMarois, P., PennerHahn, J.E., Yocum, C.F., Wright, D.W., Dube, C.E., Armstrong, W.H., Christou, G., Eppley, H.J., and Cramer, S.P. (1998) Characterization of the Mn oxidation states in photosystem II by K beta X-ray fluorescence spectroscopy. *Journal of Physical Chemistry B*, 102, 8350–8352.
- Brewer, P.G. and Spencer, D.W. (1971) Colorimetric determination of manganese in anoxic waters. *Limnology and Oceanography*, 16, 107–112.
- Burns, R.G. (1976) The uptake of cobalt into ferromanganese nodules, soils, and synthetic manganese (IV) oxides. *Geochimica et Cosmochimica Acta*, 40, 95–102.
- Burns, R.G. and Burns, V.M. (1977) Mineralogy. Marine manganese deposits, p. 185–248. Elsevier, Amsterdam.
- — — (1979) Manganese oxides. In R.G. Burns, Ed., *Marine Minerals*, vol. 6, p. 1–46. Reviews in Mineralogy, Mineralogical Society of America, Washington, D.C.
- Chukhrov, F.V., Drits, V.A., Gorshkov, A.I., Sakharov, B.A., and Dikov, Y.P. (1987) Structural models of vernadite. *International Geology Review*, 29, 1337–1347.
- Duff, M.C., Hunter, D.B., Triay, I.R., Bertsch, P.M., Reed, D.T., Sutton, S.R., Shea-Mccarthy, G., Kitten, J., Eng, P., Chipera, S.J., and Vaniman, D.T. (1999) Mineral associations and average oxidation states of sorbed Pu on tuff. *Environmental Science & Technology*, 33, 2163–2169.
- Fuller, C.C. and Harvey, J.W. (2000) Reactive uptake of trace metals in the hyporheic zone of a mining-contaminated stream, Pinal Creek, Arizona. *Environmental Science Technology*, 34, 1150–1155.
- George, G.N. (1993) EXAFSPAK. Stanford Synchrotron Radiation Laboratory, Stanford.
- Greene, A.C. and Madgwick, J.C. (1991) Microbial formation of manganese oxides. *Applied and Environmental Microbiology*, 57, 1114–1120.
- Haack, E.A. and Warren, L.A. (2003) Biofilm hydrous manganese oxyhydroxides and metal dynamics in acid rock drainage. *Environmental Science Technology* 37, 4138–4147.
- Harvey, J.W. and Fuller, C.C. (1998) Effect of enhanced manganese oxidation in the hyporheic zone on basin-scale geochemical mass balance. *Water Resources Research*, 34, 623–636.
- Hastings, D. and Emerson, S. (1986) Oxidation of manganese by spores of a marine *Bacillus*: kinetic and thermodynamic considerations. *Geochimica et Cosmochimica Acta*, 50, 1819–1824.
- Hem, J.D. (1989) Study and Interpretation of the Chemical Characteristics of Natural Water. US Geological Survey Water-Supply Paper 2254. 263 p. U.S. Geological Survey, Washington, DC.
- Hem, J.D. and Lind, C.J. (1983) Nonequilibrium models for predicting forms of precipitated manganese oxides. *Geochimica et Cosmochimica Acta*, 47, 2037–2046.
- Huang, P.M. (1991) Kinetics of redox reactions on manganese oxides and its impact on environmental quality. In D.L. Sparks, and D.L. Suarez, Eds., *Rates of Soil Chemical Processes*, p. 191–230. Soil Science Society of America, Inc., Madison, Wisconsin.
- Jenne, E.A. (1967) Controls on Mn, Fe, Co, Ni, Cu and Zn concentrations in soils and water: the significant role of hydrous Mn and Fe oxides. *Trace Inorganics in Water*, p. 337–387. American Chemical Society, Washington, D.C.
- Kuma, K., Usui, A., Paplawsky, W., Gedulin, B., and Arrhenius, G. (1994) Crystal structures of synthetic 7 and 10 angstrom manganates substituted by mono- and divalent cations. *Mineralogical Magazine*, 58, 425–447.
- Lanson, B., Drits, V.A., Silvester, E., and Manceau, A. (2000) Structure of H-exchanged hexagonal birnessite and its mechanism of formation from Na-rich monoclinic buserite at low pH. *American Mineralogist*, 85, 826–838.
- Mandernack, K.W., Post, J., and Tebo, B.M. (1995) Manganese mineral formation by bacterial spores of the marine *Bacillus* strain SG-1: Evidence for the direct oxidation of Mn(II) to Mn(IV). *Geochimica et Cosmochimica Acta*, 59, 4393–4408.
- Mann, S., Sparks, N.H.C., Scott, G.H.E., and deVrind-deJong, E.W. (1988) Oxidation of manganese and formation of Mn_3O_4 (hausmannite) by spore coats of a marine *Bacillus* sp. *Applied Environmental Microbiology*, 54, 2140–2143.
- Marble, J.C., Corley, T.L., Conklin, M.H., and Fuller, C.C. (1999) Environmental factors affecting oxidation of manganese in Pinal Creek, Arizona. In D.W. Morganwalp, and H.T. Buxton, Eds., *Water-Resources Investigation Report*, 99-4018A, p. 173–183. U.S. Geological Survey, West Trenton, New Jersey.
- McKenzie, R.M. (1980) The adsorption of lead and other heavy metals on oxides of manganese and iron. *Australian Journal of Soil Research*, 18, 61–73.
- Messinger, J., Robblee, J.H., Bergmann, U., Fernandez, C., Glatzel, P., Visser, H., Cinco, R.M., McFarlane, K.L., Bellacchio, E., Pizarro, S.A., Cramer, S.P., Sauer, K., Klein, M.P., and Yachandra, V.K. (2001) Absence of Mn-centered

- oxidation in the S-2 \rightarrow S-3 Transition: Implications for the mechanism of photosynthetic water oxidation. *Journal of the American Chemical Society*, 123, 7804–7820.
- Murray, J.W. (1974) The surface chemistry of hydrous manganese dioxide. *Journal of Colloid Interface Science*, 46, 357–371.
- Nealson, K.H. and Ford, J. (1980) Surface enhancement of bacterial manganese oxidation: Implications for aquatic environments. *Geomicrobiology Journal*, 2, 21–37.
- Nelson, Y.M., Lion, L.W., Shuler, M.L., and Ghiorse, W.C. (1999) Lead binding to metal oxide and organic phases of natural aquatic biofilms. *Limnology*, 44, 1715–1729.
- O'Reilly, S.E. and Hochella, M.F. Jr. (2003) Lead sorption efficiencies of natural and synthetic Mn and Fe-oxides. *Geochimica et Cosmochimica Acta*, 67, 4471–4487.
- Pecher, K., McCubbery, D., Kneedler, E., Rother, J., Bargar, J., Meigs, G., Cox, L., Nealson, K., and Tonner, B. (2003) Quantitative charge state analysis of manganese biominerals in aqueous suspension using Scanning Transmission X-ray Microscopy (STXM). *Geochimica et Cosmochimica Acta*, 67, 1089–1098.
- Peng, G., Degroot, F.M.F., Hamalainen, K., Moore, J.A., Wang, X., Grush, M.M., Hastings, J.B., Siddons, D.P., Armstrong, W.H., Mullins, O.C., and Cramer, S.P. (1994) High-resolution manganese X-ray fluorescence spectroscopy—oxidation-state and spin-state sensitivity. *Journal of the American Chemical Society*, 116, 2914–2920.
- Post, J.E. (1999) Manganese oxide minerals: crystal structures and economic and environmental significance. *Proceedings of the National Academy of Sciences U.S.A.*, 96, 3447–3454.
- Reynolds, R.C. Jr. (1989) Diffraction by Small and Disordered Crystals. In D.L. Bish, and J.E. Post, Eds., *Modern Powder Diffraction*, vol. 20, p. 145–182. *Reviews in Mineralogy*, Mineralogical Society of America, Washington, D.C.
- Riggs-Gelasco, P.J., Yocum, C.F., and Penner-Hahn, J.E. (1996) Reduced derivatives of the Mn cluster in the oxygen-evolving complex of photosystem II: An EXAFS study. *Journal of the American Chemical Society*, 118, 2387.
- Rosson, R.A. and Nealson, K.H. (1982) Manganese binding and oxidation by spores of a marine *Bacillus*. *Journal of Bacteriology*, 151, 1027–1034.
- Taguchi, M., Uozumi, T., and Kotani, A. (1997) Theory of X-ray photoemission and X-ray emission spectra in manganese compounds. *Journal of the Physical Society of Japan*, 66, 247–256.
- Tebo, B.M. (1991) Manganese(II) oxidation in the suboxic zone of the Black Sea. *Deep-Sea Research*, 38(Suppl. 2), S883–S905.
- Tebo, B.M., Bargar, J.R., Clement, B., Dick, G., Murray, K.J., Parker, D., Verity, R., and Webb, S. (2004) Manganese biooxides: properties and mechanisms of formation. *Annual Review of Earth and Planetary Science*, 32, 287–328.
- Tebo, B.M., Ghiorse, W.C., Van Waasbergen, L.G., Siering, P.L., and Caspi, R. (1997) Bacterially Mediated Mineral Formation: Insights into Manganese(II) Oxidation from Molecular Genetic and Biochemical Studies. In J.F. Banfield and K.H. Nealson, Eds., *Geomicrobiology: Interactions Between Microbes and Minerals*, vol. 35, p. 448. *Reviews in Mineralogy*, Mineralogical Society of America, Washington, D.C.
- Tebo, B.M., Nealson, K.H., Emerson, S., and Jacobs, L. (1984) Microbial mediation of Mn(II) and Co(II) precipitation at the O₂/H₂S interfaces in two anoxic fjords. *Limnology and Oceanography*, 29, 1247–1258.
- Tsutsumi, K., Nakamori, H., and Ichikawa, K. (1976) X-ray Mn K β emission spectra of manganese oxides and manganates. *Physical review B*, 13, 929–933.
- Urch, D.S. and Wood, P.R. (1978) The determination of the valency of manganese in minerals by X-ray fluorescence spectroscopy. *X-ray Spectrometry*, 7, 9–12.
- Villalobos, M., Toner, B., Bargar, J., and Sposito, G. (2003) Characterization of the manganese oxide produced by *Pseudomonas putida* strain MnB1. *Geochimica et Cosmochimica Acta*, 67, 2649–2662.
- Visser, E.S., McGuire, T.C., Palmer, G.H., Davis, W.C., Shkap, V., Pipano, E., and Knowles Jr., D.P. (1992) The *Anaplasma marginale msp5* gene encodes a 19-kilodalton protein conserved in all recognized *Anaplasma* species. *Infection and Immunity*, 60, 5139–5144.
- Visser, H., Anxolabehere-Mallart, E., Bergmann, U., Glatzel, P., Robblee, J.H., Cramer, S.P., Girerd, J.J., Sauer, K., Klein, M.P., and Yachandra, V.K. (2001) MnK-edge XANES and K beta XES studies of two Mn-oxo binuclear complexes: Investigation of three different oxidation states relevant to the oxygen-evolving complex of photosystem II. *Journal of the American Chemical Society*, 123, 7031–7039.
- Warren, L.A. and Haack, E.A. (2004) Microbial geoengineering: Acid rock drainage biofilms, metals, and Mn oxyhydroxides. *Geochimica et Cosmochimica Acta*, 68, A194.
- Webb, S.M. (2004) SIXPACK: a graphical user interface for XAS analysis using IFEFFIT. *Physica Scripta*, in press.
- Webb, S.M., Bargar, J.R., Dick, G.J., Johnson, H.A., McCarthy, J.K., and Tebo, B.M. (2004) Insights into the mechanism of enzymatic manganese(II) oxidation by diverse bacterial species. Presented in the Symposium on Bacterially Mediated Mn and Fe Oxidation in the Biosphere. *Geochemistry Division Abstracts of the 227th ACS National Meeting*, March 30–31, 2004., p. 62. American Chemical Society, Anaheim, California.

MANUSCRIPT RECEIVED NOVEMBER 19, 2003

MANUSCRIPT ACCEPTED AUGUST 8, 2004

MANUSCRIPT HANDLED BY KATRINA EDWARDS